Volume 17
Number 19
21 May 2025
Pages 11765-12520

Nanoscale

rsc.li/nanoscale

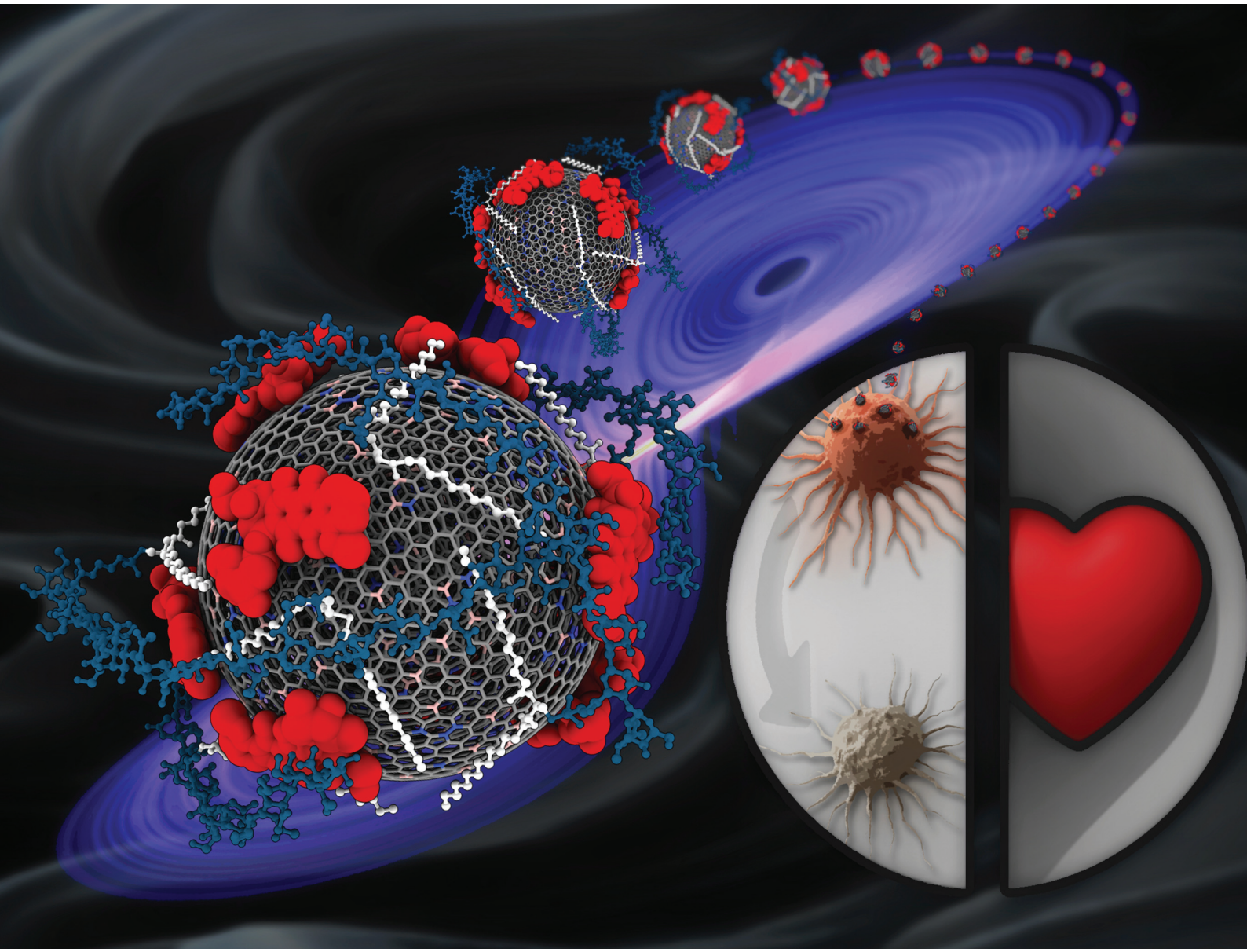

ISSN 2040-3372

ROYAL SOCIETY OF CHEMISTRY

PAPER
Silvia Arpicco, Silvia Giordani *et al.*
B/N-doped carbon nano-onions as nanocarriers for targeted breast cancer therapy

NCNST

Nanoscale

PAPER

View Article Online
View Journal | View Issue

Cite this: *Nanoscale*, 2025, **17**, 12108

B/N-doped carbon nano-onions as nanocarriers for targeted breast cancer therapy†

Hugh Mohan,[a] Iris Chiara Salaroglio,[b] Michał Bartkowski,[a] Kellyjean Courtney,[a] Ilaria Andreana,[c] Tania Limongi,[c] Raul Arenal,[d,e,f] Chiara Riganti,[b] Silvia Arpicco*[c] and Silvia Giordani *[a]

Received 28th November 2024,
Accepted 25th March 2025

DOI: 10.1039/d4nr04990j

rsc.li/nanoscale

Cancer is one of the leading causes of death worldwide and represents a significant burden on global health systems. Many existing chemotherapy treatments come with severe side effects, ranging from hair loss to cardiotoxicity, and many types of cancer express chemotherapy resistance, such as triple-negative breast cancer. This study presents a novel boron/nitrogen-doped carbon nano-onion (BN-CNO) based nanocarrier system that can deliver doxorubicin (DOX) to cancer cells *via* a pH-dependent drug release mechanism. The nanocarrier formulation consists of a hyaluronic acid/phospholipid conjugate (HA-DMPE) that is non-covalently bound to the BN-CNOs upon which DOX is loaded *via* π–π stacking interactions. The HA-DMPE/BN-CNO/DOX system enhances the uptake and anticancer effects of DOX in MDA-MB-468 and MDA-MB-231 TNBC cells whilst reducing the cardiotoxicity of DOX in AC-16 human cardiomyocytes.

1. Introduction

Resulting in over 600 000 deaths per year globally, breast cancer represents a significant burden on health systems throughout the world and is a leading cause of mortality.[1] In almost half of all cases, this disease has no specific risk factors other than age and gender. Triple-negative breast cancer (TNBC) is a type of malignancy that lacks receptors for oestrogen, progesterone, and human epidermal growth factor, making it challenging to target with therapeutic agents. TNBC accounts for 10–20% of invasive breast cancer cases and is highly invasive and prone to drug resistance, making it challenging to treat.[2]

Doxorubicin (DOX), an anthracycline antibiotic, is the most effective chemotherapy drug used to combat TNBC.[3] DOX acts by intercalating into DNA, inducing DNA damage by forming adducts and single-strand breaks. Additionally, by trapping topoisomerase II enzymes once bound to DNA, DOX further impairs DNA repair processes, ultimately leading to apoptosis.[4] As is often the case with chemotherapy treatments, DOX comes with severe side effects, the most serious of which is cardiotoxicity, which can occur due to DOX-induced apoptosis and oxidative stress.[5,6] Consequently, adverse effects restrict the dose and length of DOX regimens, limiting their clinical potential.

Nanotechnology can be leveraged to circumnavigate the toxicity of DOX (and other chemotherapy drugs)—a range of doxorubicin-based nanocarrier systems exists in the literature.[7] Carbon nanomaterials (CNMs) such as carbon nanotubes, fullerenes, carbon dots, and carbon nano-onions are often used in these systems, as they have a rich library of surface modifications available to them,[8] allowing for a range of molecules to be attached. Folic acid[9–11] and hyaluronic acid (HA)[12,13] are some of the most commonly used targeting ligands, possibly due to their small molecular size and affordability. However peptides[14] and antibodies[15] have also been used. The base nanoparticles for these systems are often oxidised to increase water solubility.[16–18] In combination with oxidation, or if pristine CNMs without covalent modification are desired, dispersants such as polyethylene glycol (PEG),[19] polydopamine,[20] and nanocrystalline cellulose[21] can be used as alternatives to achieve effective nanocarrier dispersion.

Fluorophores such as AlexaFluor™ [22] can be used to track nanocarriers during *in vitro* experiments, and a myriad of photosensitisers and drug molecules offer effective anti-

[a]*School of Chemical Sciences, Lonsdale building, Dublin City University, Dublin, Ireland. E-mail: Silvia.Giordani@dcu.ie*
[b]*Department of Oncology and Molecular Biotechnology Center "G. Tarone", piazza Nizza 44, 10126 Torino, Italy*
[c]*Department of Drug Science and Technology, Via Pietro Giuria, 9, 10125 Torino, Italy. E-mail: silvia.arpicco@unito.it*
[d]*Instituto de Nanociencia y Materiales de Aragon (INMA), CSIC-U. de Zaragoza, 50009 Zaragoza, Spain*
[e]*Laboratorio de Microscopias Avanzadas (LMA), Universidad de Zaragoza, 50018 Zaragoza, Spain*
[f]*ARAID Foundation, 50018 Zaragoza, Spain*
† Electronic supplementary information (ESI) available. See DOI: https://doi.org/10.1039/d4nr04990j

cancer payloads.[7] This enables combining cancer imaging, targeting, and treatment into a single strategy known as theragnostics.

The use of multi-functional polymers in nanocarrier systems is of great interest, as multiple functionalities can be incorporated into the polymer coating; for example, Lai *et al.* functionalised nanodiamonds with an oligo(ethylene) glycol methyl ether acrylate-based polymer that incorporated gemcitabine *via* an acid-sensitive linker to produce a pH-responsive, water-soluble anticancer nanocarrier.[23] Zhou *et al.* used a similar approach, coating carboxylated multi-walled carbon nanotubes (CNTs) with a folic acid/poly-L-lysine conjugate polymer and, subsequently, loading the nanocarrier with DOX to create a drug delivery system for the treatment of liver cancer.[24]

In our previous studies, HA-DMPE has been used to disperse pristine CNOs, which increased their solubility and showed excellent uptake in $CD44^+$ human breast carcinoma cells compared to $CD44^-$ human ovarian carcinoma cells—these HA-DMPE-coated CNOs also displayed high biocompatibility in zebrafish.[25] Of relevance to the current study, we also investigated the dispersibility properties of HA-DMPE in conjunction with BN-CNOs, finding that functionalising BN-CNOs with the HA-DMPE conjugate resulted in stable dispersions in water, even at a 10 : 1 nanoparticle-to-conjugate mass ratio.[26]

We also utilised the HA-DMPE conjugate in an HA-DMPE/CNT/DOX nanocarrier system, which was produced by non-covalently attaching HA-DMPE to CNTs and loading DOX.[27] This study is relevant as it allowed us to optimise the HA-DMPE conjugate for carbon-based nanocarriers and drug delivery applications. A range of HA molecular weights was tested, and it was found that HA-DMPE prepared from a 200 kDa HA polymer resulted in the highest cellular uptake and anticancer activity, and DOX-free HA-DMPE/CNT demonstrated excellent biocompatibility.[27]

In a separate study, we further demonstrated the viability of HA-DMPE with CNM-based nanocarriers. Functionalised nanodiamonds were shown to be biocompatible in pancreatic, breast, and lung cancer cell lines, exhibiting high uptake *via* CD44-mediated endocytosis.[28] These HA-DMPE-functionalised nanodiamonds localised within the nuclei of all three cell types, underscoring their potential as promising nanocarriers for anti-cancer drug delivery.[28]

One of the challenges, as well as a fundamental benefit of nanocarrier research, is leveraging both the intrinsic properties of the nanomaterial and incorporating multifunctional components to enhance the complexity and efficacy of these formulations. In this study, boron/nitrogen co-doped carbon nano-onions (BN-CNOs) are utilised as the core scaffold of the nanocarrier system, as detailed in Scheme 1. This material has many intrinsic benefits; it could be used for boron neutron capture therapy,[29] photothermal therapy,[30] and the presence of dopants increases the aqueous solubility of the BN-CNOs compared to undoped nano-onions.[31] Increased solubility is particularly advantageous as it allows for easier preparation of drug delivery systems. These properties can be leveraged to add another dimension of targetability and anticancer efficacy to nanocarrier systems. These multi-layered, fullerene-like nanoparticles display excellent biocompatibility in zebrafish and in NIH3T3 and MCF-7 cells.[31] Our group has developed a simple, environmentally friendly method of producing BN-CNOs in large quantities.[32]

A bioconjugate polymer consisting of HA linked to 1,2-dimyristoyl-*sn-glycero*-3-phosphoethanolamine (DMPE) is utilised in this work. The purpose of this HA-DMPE conjugate is threefold; firstly, the HA acts as a targeting ligand for the CD44 receptor, which is overexpressed in breast cancer[33] and, notably, in the case of DOX, isn't expressed in human cardiomyocytes.[34] Secondly, the phosphate groups of DMPE and oxygen-rich functionalities of HA may contribute to the improved dispersion of carbon nanomaterials. Finally, the alkyl chains of the phospholipid non-covalently anchor the polymer to the surface of CNMs *via* hydrophobic interactions. This approach prevents damage to the CNM structure, which can otherwise result from covalent modification—for example, oxidation is known to strip dopants from the surface of BN-CNOs.[31]

In this project, we enhance the BN-CNO nanocarrier scaffold by incorporating doxorubicin (DOX) alongside the HA-DMPE conjugate, leveraging previously discussed benefits. The inclusion of DOX introduces a pH-sensitive drug-release control mechanism. This system exploits the acidic microenvironment of cancer cells, which results from increased CO_2 and lactic acid production.[35] Under acidic conditions, the amine group of DOX becomes highly protonated, increasing its positive charge and hydrophilicity, leading to its release from the BN-CNO surface. In contrast, DOX remains less charged in neutral physiological conditions and stays bound to the nanocarrier, allowing for controlled drug retention.

In summary, in this study, we further expand on our nanocarrier research by preparing, characterising and investigating the HA-DMPE/BN-CNO/DOX nanocarrier for the targeted delivery of DOX to CD44 overexpressing cancer cells. The therapeutic efficacy of this nanocarrier was compared to both free DOX and Caelyx®—a PEGylated liposomal formulation of DOX approved by the European Medicines Agency (EMA) in 1996[36] to assess its performance in DOX uptake and anticancer activity assays. This comparison allows us to evaluate the potential of the HA-DMPE/BN-CNO/DOX nanocarrier as a more effective alternative to current DOX formulations.

The Caelyx® formulation has many benefits over free DOX, enhancing its pharmacokinetic profile and increasing its circulation time. This results in increased tumour DOX concentration and, therefore, higher efficacy than free drug. The main drawback of liposomal DOX formulations is their poor stability.[37] This is an issue that can be overcome by CNM-based nanocarriers, which are very stable. Another benefit of CNM-based nanocarriers is the vast range of covalent and non-covalent functionalisation options available, allowing for a range of targeting, drug, and tracking moieties to be incorporated into these systems.

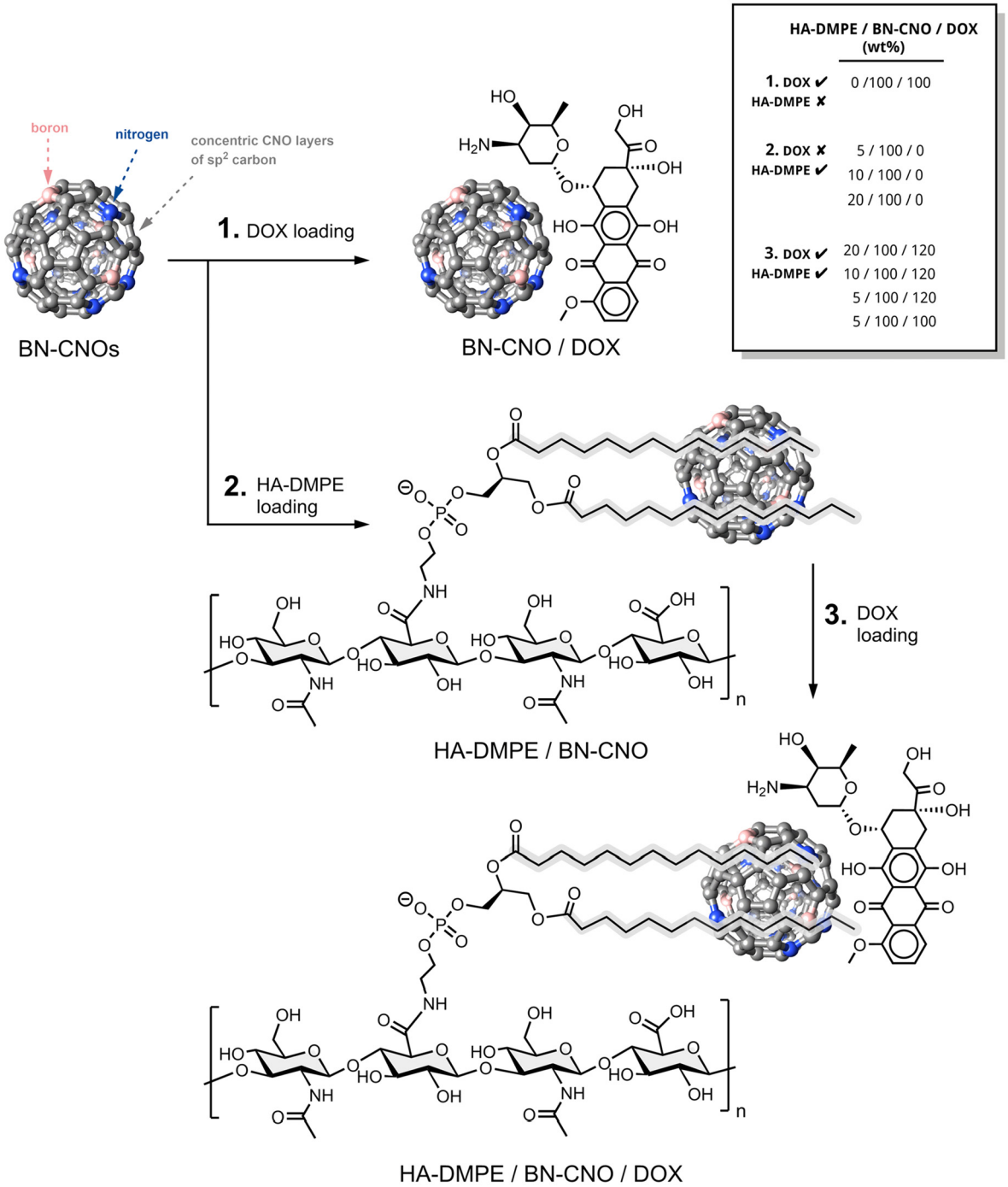

Scheme 1 Nanocarrier preparation|(1) DOX-loading of BN-CNOs to prepare the HA-DMPE-free BN-CNO/DOX; (2) HA-DMPE-loading of BN-CNOs to prepare the DOX-free HA-DMPE/BN-CNOs; and (3) the subsequent DOX-loading of HA-DMPE/BN-CNOs to prepare HA-DMPE/BN-CNO/DOX. All wt% ratios of the BN-CNO-based nanocarriers formulated and investigated in this study are tabulated in the inset. Procedures and experimental conditions for the loading processes are detailed in the Materials and Methods section.

2. Experimental

2.1 Materials

Detonation nano-diamond powder (uDiamond® Molto, 4.2 ± 0.5 nm crystal size) was purchased from Carbodeon (Pakkalankuja, Finland). Boric acid (≥99.5%) and all buffers were purchased from Sigma Aldrich (Arklow, Ireland). DMSO (99.9%, for spectroscopy) was purchased from Thermo Fischer Scientific (Dublin, Ireland). The phospholipid 1,2-dimyristoyl-*sn*-glycero-3-phosphoethanolamine (DMPE) was purchased from Merck (Milan, Italy). 200 kDa sodium hyaluronate (HA) was purchased from Lifecore Biomedical (Chaska, MN, USA),

and doxorubicin hydrochloride (DOX·HCl) was purchased from TCI Europe N.V. (Zwijndrecht, Belgium). The HA-DMPE conjugate was synthesised as previously described, specifically utilising HA of 200 kDa molecular weight.[25]

Boron/nitrogen co-doped carbon nano-onions (BN-CNOs) were synthesised by thermally annealing a mixture of detonation nanodiamonds (DNDs) and boric acid under an inert atmosphere.[32] Briefly, DNDs and boric acid (30% w/w) were homogenised through vigorous shaking in a glass vial. The resulting mixed powder was then placed in a graphite crucible and heated to 1650 °C for 1 h in a GSL-1750X-KS-UL tube furnace (MTI Corporation) under He. The material was then air-annealed at 450 °C for 4 h in a KSL-1200X-J box furnace (MTI Corporation).

2.2 HA-DMPE/BN-CNO nanocarrier preparation

BN-CNOs were non-covalently functionalised with HA-DMPE to prepare HA-DMPE/BN-CNOs of desired wt% ratios. Briefly, BN-CNOs (5 mL, 1 mg mL^{-1}) were dispersed with HA-DMPE in deionised water by sonication for 1.5 h in an Elmasonic S30 ultrasonic bath. The water temperature in the sonicator was maintained at <30 °C. The dispersion was then centrifuged in a glass centrifuge tube at 400 RCF for 5 min (Yingtai Instrument Co. TG16). The top 4 mL was carefully taken and checked by dynamic light scattering (DLS) to confirm the removal of large aggregates, and by UV-vis absorption spectroscopy to determine the BN-CNO concentration. The dispersion was then diluted with 0.01 M pH 7.4 PBS to form a 20 mL solution with a BN-CNO concentration of 125 μg mL^{-1}, and this solution was then sonicated for a further 15 min. A black dispersion of HA-DMPE/BN-CNOs was obtained.

2.3 DOX loading and quantification

DOX was then loaded onto the HA-DMPE/BN-CNO nanocarrier by adding DOX to the sonicated black dispersion of HA-DMPE/BN-CNOs and stirring in the dark at room temperature for 72 h. The HA-DMPE/BN-CNO/DOX nanocarrier dispersion was then transferred to a glass centrifuge tube and centrifuged at 10 000 RCF for 5 min, following which the supernatant was decanted and retained. This process was repeated with 3 × 20 mL PBS washings. All the washings were combined, and the amount of unbound DOX was quantified by UV-vis spectroscopy by measuring the absorption intensity at 480 nm. For drug release studies, UV-vis absorption spectroscopy, DLS and ZP analysis, the reddish-black sediment was immediately redispersed in buffer/deionised water by sonicating for 1 min and shaking. For all other analyses, the sediment was dried in a vacuum oven at 40 °C for 16 h to yield a powder.

The final HA-DMPE/BN-CNO/DOX nanocarrier was prepared at different wt% ratios of the individual components. In summary, the following wt% formulations were prepared and investigated: 20/100/120, 10/100/120, 5/100/100. Control formulations containing no DOX, or no HA-DMPE, were also prepared. Regarding the DOX-free HA-DMPE/BN-CNOs, the wt% formulations of 20/100/0, 10/100/0 and 5/100/0 were prepared. Regarding the HA-DMPE-free control, a wt% formulation of BN-CNO/DOX of 0/100/100 was prepared.

From the UV-vis absorption spectroscopy analyses, drug loading efficiency (DLE) and drug loading content (DLC) were calculated using eqn (1) and (2).

$$\mathrm{DLE}\,(\%) = \frac{\text{amount of loaded drug}}{\text{total amount of drug used in loading}} \times 100 \quad (1)$$

$$\mathrm{DLC}\,(\mathrm{wt}\%) = \frac{\text{mass of loaded drug}}{\text{mass of drug-loaded nanocarrier}} \times 100 \quad (2)$$

2.4 Physicochemical characterisation

All UV-vis absorbance characterisation was performed on a Shimadzu UV-2600 instrument with 1 cm path-length quartz cuvettes. Samples were diluted to 5 μg mL^{-1} in deionised water and sonicated for 5 min. Background correction was performed.

Attenuated total reflection Fourier-transform infrared spectroscopy (ATR-FTIR) was carried out on a Thermo Fischer Scientific Nicolet™ Summit™ FTIR instrument with an Everest ATR accessory containing a diamond crystal and a DTGS KBr window detector, with measurements taken at room temperature, and background correction performed immediately prior to analysing each material. The spectra were recorded with a resolution of 0.482 cm^{-1}, accumulating 64 scans per sample for DOX and HA-DMPE, and 128 scans for bare and functionalised BN-CNO nanomaterials. Norton Beer Strong apodization and atmospheric suppression were automatically applied, with an airPLS baseline correction applied to the spectra of all BN-CNO materials[38] (lambda parameter set to 3000).

DLS and zeta potential (ZP) analyses were performed using a Malvern Zen 3600 ZetaSizer in backscattering mode (173°); quartz and disposable ZP cuvettes were used for DLS and ZP, respectively. Samples were diluted to 5 μg mL^{-1} in deionised water and sonicated for 5 min. Samples were equilibrated to 25 °C and measured in triplicate, with each sample subjected to individual measurement cycles of at least 1 min.

X-ray photoelectron spectroscopy (XPS) was carried out on an AXIS Supra instrument (Kratos Analytical, UK) equipped with a 120 W Al Kα (1486.6 eV) monochromatic source. Samples were deposited on an Si substrate and spectra were calibrated using the C 1s peak. Survey and core level spectra were acquired using 160 eV and 20 eV pass energy, respectively. Data was processed with CasaXPS v23.3 software, with peak fitting carried out using the Lorentzian function after Tougaard background subtraction. Quantification was carried out using Kratos RSF software. Data was plotted using Origin. Additionally, the survey spectra of the DOX-loaded nanocarriers revealed the presence of fluorine (Fig. S4C–E†). Specifically, an F 1s peak at 688.9 eV, which is highly characteristic of the $-CF_2$ bonding environment, and an F Auger peak was also observed at 835 eV. These signals originated from the PTFE-lined caps of the amber vials used to protect the light-sensitive DOX in the DOX-loaded materials. Silicon contri-

butions were also observed in the 20/100/0 wt% HA-DMPE/BN-CNO/DOX survey spectrum (Fig. S4B†), specifically Si 2p and Si 2s peaks, present at 101 eV and 152 eV, respectively. These signals originated from the silicon substrate used for the XPS analysis. Due care was taken to exclude the F and Si contributions from the quantitative interpretation of the data.

A Bruker ICON instrument operating in PeakForce Tapping™ mode utilising ScanAsyst Air™ optimisation was used for AFM analysis. Solid samples were dispersed in DMSO at 5 μg mL^{-1} by sonicating for 5 min. These were drop-cast onto freshly cleaved mica and dried on a 70 °C hotplate for 5 min. The mica had previously been attached to a glass microscopy slide using superglue. Glass pipettes, Petri dishes and vials were used to prevent nanoplastic contamination. Samples were analysed immediately under ambient conditions using Bruker ScanAsyst Air HPI tips (0.25 N m^{-1} spring constant, 55 kHz resonance frequency, 2 nm tip radius), and the *z*-axis of the instrument was calibrated using a 21 nm standard (Bruker). All AFM images were taken using NanoScope software and are 500 nm × 500 nm. The scan rate and samples/line were set to 2 Hz and 208, respectively. Gwyddion software was used for image processing. Each micrograph was levelled by fitting a plane through three points and corrected using step line correction. Individual particles were selected using the mask function, and grain distributions were exported to Origin for size distribution analysis.

HRTEM images were taken using an image-corrected ThermoFisher Scientific Titan Cube instrument with an operating voltage of 80 kV and in a ThermoFisher Scientific Tecnai F30 working at 300 kV. HAADF-STEM images were acquired using a probe-corrected Titan low-base instrument equipped with a high-brightness gun (X-FEG) and operating at 120 keV. Convergence angle was 25 mrad, and acceptance angle was 48 mrad. Samples were dispersed in deionised water and deposited on a holey carbon film supported by a copper TEM grid before drying at ambient temperature.

2.5 DOX release studies

DOX release was performed in triplicate, with independent experiments carried out in both 0.01 M pH 7.4 PBS, and 0.01 M pH 5.2 sodium acetate buffer, at 37 °C. Briefly, a portion of the selected buffer and a brown glass vial were allowed to equilibrate in a water bath. The nanocarrier was dispersed in 10 mL of equilibrated buffer in the vial by sonicating for 1 min and shaking; a stir bar was added, and the vial was returned to the water bath and stirred at 600 rpm. 1 mL aliquots were sampled at a series of time points—specifically, samples were taken at 0.5, 1, 2, 3, 6, 24, 48, and 72 h, with 96 and 120 h data points included for the extended studies of the 20/100/120 wt% HA-DMPE/BN-CNO/DOX formulation. The vial was removed from the water bath, shaken, and 1 mL was abstracted and transferred to a glass centrifuge tube. 1 mL of equilibrated buffer was added to the vial to keep the volume at 10 mL. The vial was then shaken and put back in the water bath. 1 mL of buffer was also added to the sample in the centrifuge tube. This sample was centrifuged at 10 000 RCF for 5 min. The top 1 mL was carefully taken, and the concentration of the released DOX was determined by UV-vis spectroscopy at 480 nm. The absorbance at 675 nm was subtracted from the entire spectrum to remove interference from any remaining BN-CNOs. Finally, drug release efficiency (DRE), reported as a mean ± standard deviation of the three independent experiments, was determined using eqn (3).

$$\text{DRE}\ (\%) = \frac{\text{amount of drug released}}{\text{amount of drug loaded}} \times 100 \qquad (3)$$

2.6 *In vitro* studies

2.6.1 Cell culture. Human breast cancer cell lines MCF-7, MDA-MB-468, MDA-MB-231, and human cardiomyocytes AC16 were purchased from ATCC (Manassas, VA). Cells were grown in DMEM medium, supplemented with 10% v/v fetal bovine serum (FBS) and 1% penicillin–streptomycin in a humidified atmosphere at 37 °C, 5% CO_2.

2.6.2 CD44 receptor expression. The expression of the CD44 cell surface receptor was evaluated by flow cytometry as previously described.[39] 1×10^6 cells were rinsed and fixed with 2% w/v paraformaldehyde (PFA) for 2 min, washed three times with PBS and stained with the anti-CD44 antibody (Abcam, Cambridge, UK; dilution: 1 : 50) for 1 h on ice, followed by an AlexaFluor 488-conjugated secondary antibody (Millipore, Burlington, MA; dilution: 1 : 100) for 30 min. 1×10^5 cells were analysed with EasyCyte Guava™ flow cytometer (Millipore), equipped with the InCyte software (Millipore). Control experiments included incubation with a non-immune isotype antibody.

2.6.3 Cellular uptake. 1×10^5 cells were seeded into a 96-well black plate, left untreated (control condition) or incubated for 1, 3, 6, and 24 h with free DOX, Caelyx®, 20/100/0 wt% HA-DMPE/BN-CNO, or various HA-DMPE/BN-CNO/DOX formulations with equivalent DOX concentrations of 1 nM, 10 nM, 100 nM, 1 μM, and 10 μM. For competition assays, cells treated with 20/100/120 wt% HA-DMPE/BN-CNO/DOX were co-incubated for 24 h with 200 μg mL^{-1} HA (CA, as competitor) or an anti-CD44 blocking antibody (CB, as inhibitor) diluted 1/10 in the culture medium. Cells were washed twice with 300 μL PBS, resuspended in 400 μL ethanol/HCl 0.3 N (1 : 1 v/v), and sonicated (10 bursts of 1 s, Labsonic Sonicator, Aubergne, France). A 50 μL aliquot was used to measure the intracellular content of proteins with the BCA kit (Sigma-Merck). The remaining sample was used to read the intracellular fluorescence of DOX, taken as an index of drug uptake, using a Synergy HT Microplate Reader (Bio-Tek Instruments), an excitation wavelength of 485 nm, and an emission wavelength of 553 nm. Results were expressed as nmol mg^{-1} cellular proteins, according to a titration curve of doxorubicin previously set.

2.6.4 *In vitro* toxicity. 1×10^4 cells were seeded into a 96-well white plate, left untreated (control condition) or incubated for 24, 48, or 72 h with free DOX, Caelyx®, the DOX-free 20/100/0 wt% HA-DMPE/BN-CNOs, or various HA-DMPE/BN-CNO/DOX formulations with a final equivalent DOX con-

centration of 1 nM, 10 nM 100 nM, 1 μM, 10 μM. For extended studies with the 20/100/120 wt% HA-DMPE/BN-CNO/DOX formulation, incubation times of 96 and 120 hours were also used. To ensure DOX equivalence in the DOX-free 20/100/0 wt% formulation, the samples were diluted in cell culture medium to match the BN-CNO concentration of the DOX-loaded formulations. The competition assays were conducted as described in the section detailing cellular uptake procedures. Cell viability was measured by the ATPlite Luminescence Assay System (PerkinElmer, Waltham, MA), as per the manufacturer's instructions. Results were analysed by a Synergy HT Microplate Reader (Bio-Tek Instruments, Winooski, VT). The luminescence units of the untreated cells were considered 100%; the luminescence units of the other experimental conditions were expressed as percentages *versus* untreated cells.

To measure cell necrosis, the release of lactic dehydrogenase (LDH) in the extracellular medium was measured, as previously reported.[40] The cell culture medium was centrifuged at 12 000 RCF for 15 min to remove cellular debris. Cells were washed twice with PBS, detached with 0.1 mL mL^{-1} trypsin/EDTA, resuspended in 0.2 mL of 82.3 mM triethanolamine phosphate-HCl (pH 7.6), and sonicated on ice with two 10 sec bursts. LDH activity was measured in 50 μL supernatant and 5 μL cell lysates, incubated for 6 min at 37 °C with 20 mM pyruvic acid and 5 mM NADH. The rate of NADH oxidation was followed by measuring the absorbance at 340 nm using a Synergy HT Microplate Reader. Both intracellular and extracellular enzyme activities were expressed as mmol NADH oxidised/min/dish: extracellular LDH activity was expressed as a percentage of the total (intracellular + extracellular) LDH activity.

2.6.5 Statistical analysis. All biological data is reported as mean ± standard deviation of three independent experiments. The results were analysed by a one-way ANOVA with *post hoc* Tukey's test. For cell viability and uptake studies, significance was determined using the following thresholds: $^{*}p < 0.05$, $^{**}p < 0.01$, and $^{***}p < 0.001$ indicate significant differences compared to DOX alone, while $^{\circ}p < 0.05$, $^{\circ\circ}p < 0.01$, and $^{\circ\circ\circ}p < 0.001$ denote significant differences compared to Caelyx®.

Control studies for cellular uptake and cellular viability were conducted for all analyses; however, due to the volume of the *in vitro* results presented in the article and ESI,† they are not shown in full. However, for clarity, control data is included in Fig. 4A. Competitive co-incubations with excess HA or an anti-CD44 blocking antibody (CA and CB, respectively) were also conducted and presented in all relevant cellular uptake and viability studies to assess the specificity of CD44-mediated uptake.

The DLE, DLC, pH 5.2 DRE, and pH 7.4 DRE of all formulations (three replicates each) were analysed using principal component analysis (PCA). Origin software was used for this analysis; each data point was expressed as %, with % HA-DMPE being the controlled variable. The data was normalised using a standard scalar and a correlation matrix was constructed. Eigenvalues were computed from this correlation matrix and two eigenvectors were identified to be responsible for much of the variance (96.73%), eigenvectors were extracted from these two eigenvalues and used to produce a biplot with DLE, DLC, pH 5.2 DRE, and pH 7.4 DRE represented as vectors and each sample represented as a point.

3. Results and discussion

3.1 Nanocarrier preparation

The first step in the synthesis of this nanocarrier was the non-covalent functionalisation of BN-CNOs with the HA-DMPE conjugate polymer through a simple, environmentally friendly sonication procedure. A non-covalent approach was taken to avoid using toxic solvents and reagents. This one-step functionalisation was performed in water and did not require any purification/removal of byproducts. The multifunctional biocompatible polymer imparts dispersibility and targetability to the BN-CNOs, allowing them to seek CD44 overexpressing cancer cells. A HA molecular weight of 200 kDa was chosen as this was previously found to be optimal for cancer cell targeting.[27]

BN-CNOs were produced by thermally annealing detonation nanodiamonds in the presence of boric acid. This step is also environmentally friendly as it requires no solvents and does not produce waste products. A second annealing step in air was performed to remove any amorphous carbon impurities.

DOX was then reversibly attached to the polymer-coated BN-CNOs to form the HA-DMPE/BN-CNO/DOX nanocarrier system; various ratios of polymer and drug were tested to find the optimal composition. The anthracycline backbone of the DOX was leveraged to non-covalently load the drug onto the BN-CNO surface *via* π–π stacking interactions. The primary amine on DOX allows for pH-triggered release, as it is protonated at the low pH of cancer cells.[35] This increases its solubility and causes it to be released from the nano-onion.

3.2 Physicochemical characterisation

The assembled nanocarrier was then analysed by DLS, UV-vis absorption and ATR-FTIR spectroscopy, AFM, HRTEM, and HAADF-STEM to confirm HA-DMPE and DOX functionalisation and determine its physicochemical properties.

The UV-vis absorption spectra, presented in Fig. S1,† highlight the optical properties of the individual components (DOX, HA-DMPE) and the DOX-free and DOX-loaded nanocarriers; 20/100/0 and 20/100/120 wt%, respectively. The UV-vis spectrum of the DOX-free 20/100/0 formulation shows significant absorption across the whole range, with a band concentrated at 256 nm corresponding to the $\pi \rightarrow \pi^{*}$ electronic transition of C=C bonds. An additional absorption maximum is observed at 210 nm in the DOX-loaded system due to $\pi \rightarrow \pi^{*}$ transitions from additional C=C bonds in the anthracycline backbone of the drug molecule. Drug loading also imparts two weak absorption bands at 505 nm and 549 nm, resulting from $n \rightarrow \pi^{*}$ transitions due to the C=O groups of the DOX. The 20/100/120 wt% HA-DMPE/BN-CNO/DOX formulation strongly

absorbs across the whole UV-vis range, indicating the material remains well dispersed. Interestingly, upon attachment to the BN-CNO surface, the 217 nm $\pi \rightarrow \pi^*$ and 477 nm/497 nm $n \rightarrow \pi^*$ peaks from the DOX are blue-shifted and red-shifted, respectively. This confirms attachment *via* π–π stacking interactions and results from the orbital overlap between the DOX and the BN-CNO surface.

The non-covalent HA-DMPE surface functionalisation and DOX loading were further confirmed by ATR-FTIR (Fig. S2†). In contrast to the bare BN-CNOs, hydroxyl bending vibrations are observed at 1430 cm^{-1} in the 20/100/0 and 20/100/120 wt% formulations, resulting from the presence of HA-DMPE. The fully assembled 20/100/120 nanocarrier displays N–H bending at 1570 cm^{-1} and C–O stretching at 753 cm^{-1} from DOX and HA-DMPE functionalisation.

The DLS and ZP values (Table 1) and spectra (Fig. S3†) reveal noticeable size differences between drug-loaded and drug-free formulations. This could be explained by the ~50% increase in ZP observed across all formulations upon DOX loading. The positively charged DOX shields the negative charges on the BN-CNOs surface and the phosphate and carboxyl groups of the HA-DMPE.

Loading DOX onto the DOX-free 20/100/0, 10/100/0 and 5/100/0 wt% HA-DMPE/BN-CNO formulation resulted in a size increase, with a size trend inversely proportional to the HA-DMPE content. This can be expected as the HA-DMPE conjugate aids in stabilising the dispersion.

The 20/100/0 and 10/100/0 HA-DMPE/BN-CNO formulations exhibit hydrodynamic diameters of 280 ± 93 nm and 483 ± 169 nm, respectively. Although these formulations have similar surface charges (Table 1), the difference in hydrodynamic diameter suggests that HA-DMPE disperses the nanocarrier *via* both steric and electrostatic repulsion. This is further supported by observations in the 20/100/120 wt% HA-DMPE/BN-CNO/DOX and 10/100/120 formulations, where the latter shows a significantly larger size (719 ± 593 nm *vs.* 411 ± 125 nm) despite similar ZP values (−7.8 ± 1.8 mV and −7.3 ± 0.1 mV for 20/100/120 and 10/100/120, respectively). The intricate relationship between nanoparticle surface chemistry and solution dynamics means there is no straightforward linear correlation between HA-DMPE content and hydrodynamic diameter.

Table 1 DLS and ZP studies|hydrodynamic diameter (d) and zeta potential (ZP) values of HA-DMPE/BN-CNO/DOX formulations (5 μg mL^{-1} in deionised water). The hydrodynamic diameters represent a number percentage distribution mean, and all values represent a mean ± standard deviation of $n \geq 3$ measurements

HA-DMPE/BN CNO/DOX (wt%)	*d* (nm)	ZP (mV)
20/100/0	280 ± 93	−13.6 ± 1.2
20/100/120	411 ± 125	−7.8 ± 1.8
10/100/0	483 ± 169	−15.2 ± 1.0
10/100/120	719 ± 593	−7.3 ± 0.1
5/100/0	300 ± 104	−19.2 ± 0.8
5/100/100	424 ± 117	−10.4 ± 0.2
0/100/100	200 ± 49	−14.6 ± 1.2
	793 ± 262	

The XPS survey spectrum of BN-CNOs (Fig. S4A†) confirmed the presence of boron (B 1s; 190 eV), carbon (C 1s; 284.5 eV), nitrogen (N 1s; 398 eV), and oxygen (O 1s; 532 eV); these elements were observed in all samples. Elemental analysis (Table S1;† all samples) revealed that BN-CNOs contained 6.5% O, 4.1% N, and 3.7% B. The high-resolution core-level C 1s XPS spectrum of BN-CNOs is displayed in Fig. 1A and the corresponding chemical states and percentage contributions for BN-CNOs and all other samples for C 1s are detailed in Table S2† for B 1s and Cl 2p in Table S3,† and for N 1s and O 1s in Table S4.† The C 1s spectrum shows over 80% sp^2 C, the majority of which is in the inner fullerene-like layers, which are sp^2 in nature.[41] A small amount of C (6%) is sp^3 hybridised, these are likely the atoms adjacent to defect sites containing B/N/O. The rest of the carbon in the BN-CNOs is bound to O and N, with a strong (9%) π–π* contribution confirming the presence of de-localised electrons within the BN-CNOs. The B 1s spectrum of BN-CNOs reveals that the highest proportion of B (49%) is bonded with O, followed by N (34%), then C (17%). The absence of a π–π* shake-up satellite adjacent to the B 1s and N 1s lines rules out hexagonal BN,[42] implying the B is evenly incorporated into the hexagonal CNO lattice. The N 1s spectrum shows that the majority of the nitrogen (63%) is pyridinic in nature,[43] whilst 31% of the nitrogen is bonded to B, in the form of B–N–C bonds.[44] The remainder of the N contribution is split between pyrrolic and graphitic environments, which can be expected given the sp^2 lattice structure of the BN-CNO surface. A discussion of the effects of HA-DMPE functionalisation on the XPS spectra of the 20/100/0 sample can be found in the ESI.†

Loading DOX further increases the complexity of the XPS spectra, as can be seen in the case of the 20/100/120 wt% HA-DMPE/BN-CNO/DOX sample. The survey spectrum and elemental analysis of this sample (Fig. S4E and Table S1†) confirm a 4.5% increase in O compared to DOX-free HA-DMPE/BN-CNOs and the addition of a Cl 2p contribution (199 eV, 0.5 at%) from the chloride counterion of the DOX hydrochloride salt. A small Na 1s peak was observed at 1071 eV, this is from the sodium present in the PBS buffer used in DOX functionalisation. The high-resolution core level C 1s spectrum of the 20/100/120 wt% sample (Fig. 1C) exhibits differential charging at 282.9 eV, possibly due to its insulating properties. An 18% decrease in sp^2 carbon and a 4% decrease in sp^3 carbon is observed upon loading DOX onto the HA-DMPE/BN-CNOs. This corresponds to a 5% increase in C bound to O/N from the C and O-containing groups in the DOX and dilution from the differential charging feature. A 0.5% increase in the π–π* contribution is observed, from the DOX anthracycline backbone. A small (2.5%) B–B contribution at 188 eV was observed in the B 1s spectrum of the 20/100/120 sample. The rest of the B was present as B–C (13%), B–N (51%), and B–O (33%), like the pristine BN-CNOs. The Cl contribution was split between Cl–Na (196.5 eV, 20%) and Cl–H (198.3 eV/199.9 eV, 80%). The 20/100/120 N 1s spectrum displays a 36% reduction in N–B contribution compared to HA-DMPE/BN-CNOs, with a pyridinic N peak at 398.2 eV

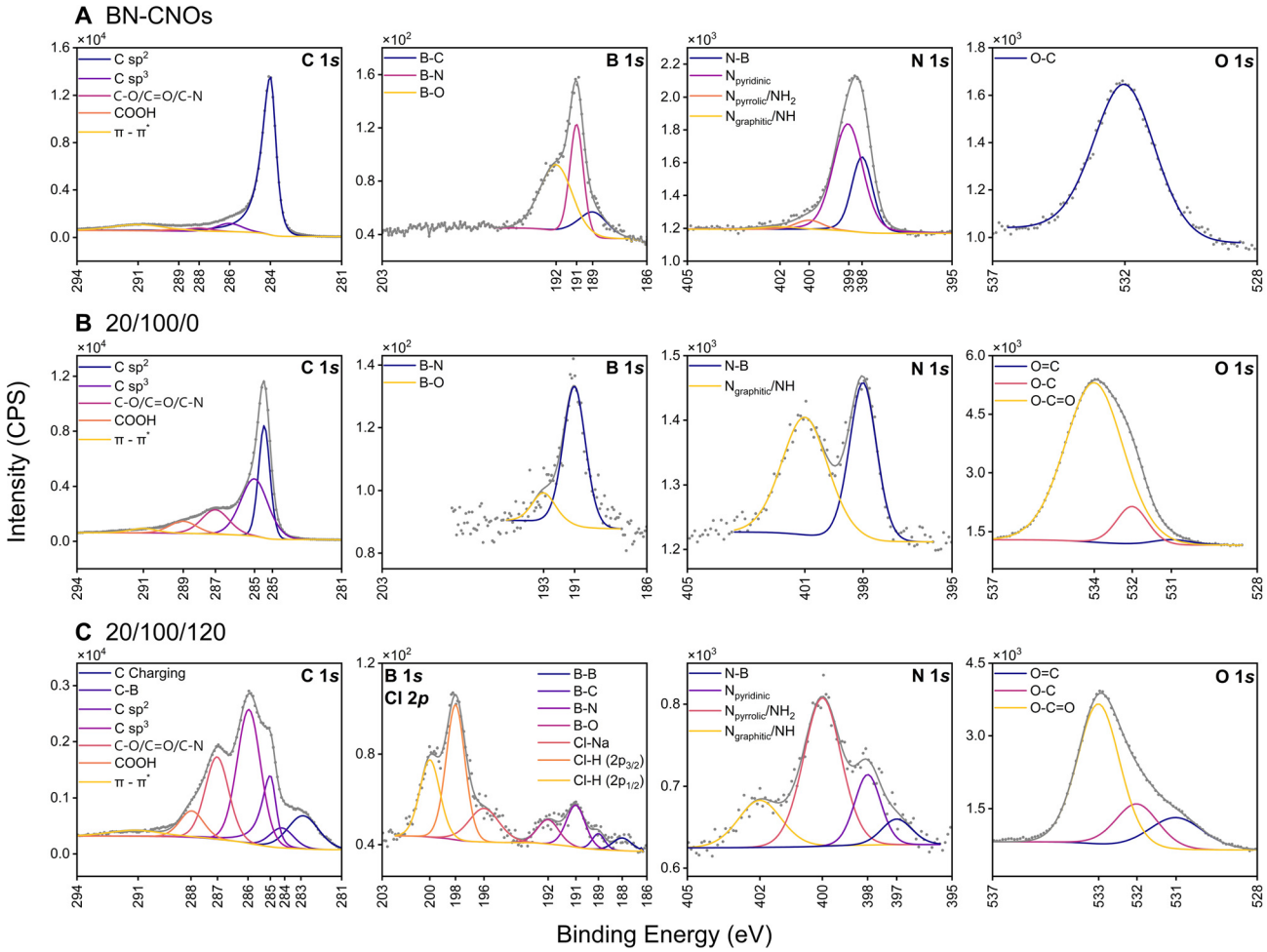

Fig. 1 XPS studies | High-resolution core level XPS spectra of (A) BN-CNOs (top row; C 1s, B 1s, N 1s, and O 1s); (B) the 20/100/0 wt% HA-DMPE/BN-CNO/DOX formulation (middle row; C 1s, B 1s, N 1s, and O 1s); and of (C) the 20/100/120 wt% HA-DMPE/BN-CNO/DOX formulation (bottom row; C 1s, B 1s & Cl 2p, N 1s, and O 1s). Spectra include experimental data (grey, scatter) and the fitted peak deconvolution envelope (grey, line).

accounting for 18.1% of the N present. The majority (54%) of the N is present as pyrrolic/NH_2 groups resulting from the BN-CNOs themselves and the DOX, respectively. Whilst the increased O content contributes to the solubility of the nanocarrier, the primary amine groups can be easily protonated, increasing the overall surface charge of the system. The increased solubility of DOX upon protonation of this amine is exploited for pH-triggered release. A 36% decrease in the $N_{graphitic}$/NH contribution is observed upon DOX loading, owing to the extra NH_2 groups from the DOX. The O 1s spectrum of the 20/100/120 wt% formulation is similar to DOX-free 20/100/0 wt% formulation, with 16% and 8% increases in O═C and O–C contributions diluting the O–C═O contribution to 63%, this is due to the extra hydroxyl and carbonyl groups of the DOX.

XPS survey spectra, elemental analysis, high-resolution C 1s, B 1s/Cl 2p, N 1s, and O 1s spectra, and contribution details from high-resolution spectra for the 5/100/100 and 10/100/120 samples can be seen in Fig. S4, Table S1, Fig. S5 and Tables S2–S4,† respectively. Trends were observed in the changes of elemental composition with increasing HA-DMPE and DOX content. O content increases with more DOX and HA-DMPE being added, this affects the surface charge and drug release kinetics of the nanocarrier. A sharp decrease in the ratio of sp^2/sp^3 C is seen with increased functionalisation, along with a reduction in π–π* contribution.

Atomic force microscopy (AFM) was used to analyse both BN-CNOs and the functionalised nanocarrier comprising 20/100/120 wt% HA-DMPE/BN-CNO/DOX to assess the impact of functionalisation on particle size and aggregation. Representative AFM micrographs are shown in (Fig. 2A and B) with corresponding line profiles shown in (Fig. 2C and D). Size distribution analysis has also been carried out over a series of micrographs to assess the comprehensive nanoparticle size in the bulk composition. Size distribution results are shown in (Fig. 2E and F), and additional AFM micrographs are shown in (Fig. S6†)

The mean height of BN-CNOs from AFM analysis was 6.79 ± 1.46 nm (n = 500). Their small size and low polydispersity make them excellent nanocarrier scaffolds, as they are small

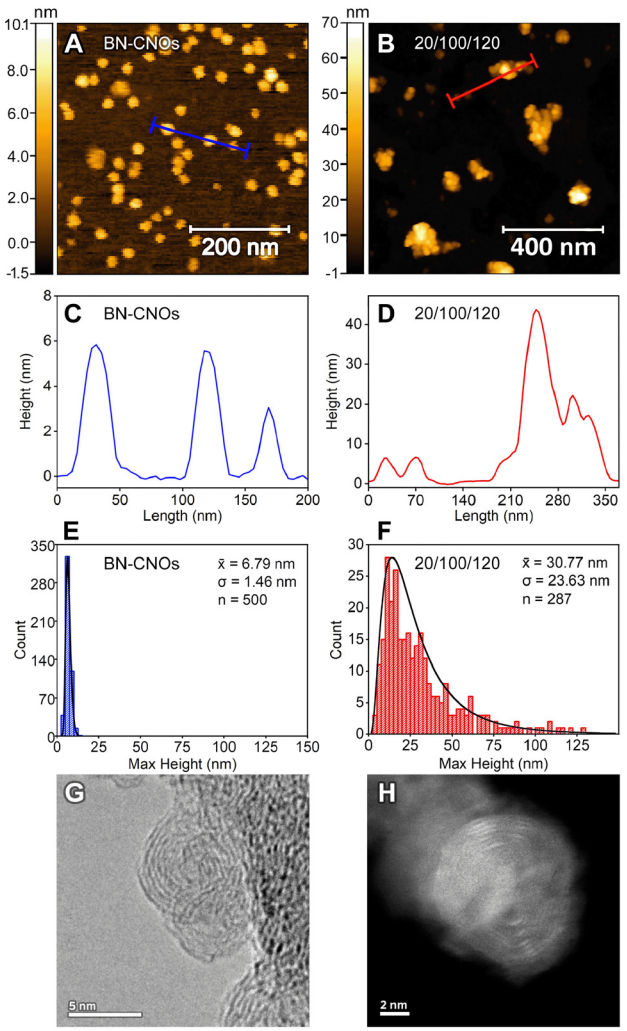

Fig. 2 AFM, HRTEM and HAADF-STEM studies|AFM micrograph of (A) BN-CNOs and (B) 20/100/120 wt% HA-DMPE/BN-CNO/DOX; their respective line profiles (C & D); and their respective size distributions (E & F). Electron microscopy studies depicting a HRTEM image of BN-CNOs (G), and a HAADF-STEM image of the 20/100/120 wt% HA-DMPE/BN-CNO/DOX formulation (H).

enough to enter cells.[45,46] Functionalisation with HA-DMPE and DOX at a wt% ratio of 20/100/120, the HA-DMPE/BN-CNO/DOX nanocarrier resulted in an expected increase in mean height, measured at 30.77 ± 23.63 nm (n = 287). Whilst examples of single functionalised BN-CNOs can be seen in the AFM line profile of HA-DMPE/BN-CNO/DOX, the majority of the nanocarrier consists of aggregates containing multiple BN-CNOs held together by large chains of HA-DMPE.

The HRTEM image of BN-CNOs (Fig. 2G) highlights the multilayered structure of the material. As seen in the HAADF-STEM image (Fig. 2H), the multilayered structure is retained in the 20/100/120 wt% HA-DMPE/BN-CNO/DOX system.

3.3 DOX loading and release

The loaded DOX was quantified by UV-vis spectroscopy, and the values are reported in Table 2. DLE, DLC, and DRE values

Table 2 Drug loading and release studies|DLC, DLE, and DRE values of noted HA-DMPE/BN-CNO/DOX wt% formulations. The values represent a mean of triplicate independent experiments ± standard deviation

HA-DMPE/ BN-CNO/DOX (wt%)	DLC (wt%)	DLE (%)	DRE@pH 7.4 (%)	DRE@pH 5.2 (%)
20/100/120	36.6 ± 1.4	57.3 ± 1.4	6.7 ± 0.6	84.0 ± 4.8
10/100/120	36.0 ± 1.4	51.3 ± 1.7	7.7 ± 0.3	37.7 ± 1.7
5/100/100	44.7 ± 0.5	92.0 ± 1.5	4.8 ± 1.0	48.3 ± 8.4
0/100/100	48.7 ± 0.0	96.7 ± 0.9	5.6 ± 0.5	14.0 ± 0.8

were calculated as per eqn (1), (2) and (3), respectively. The best DLC value achieved was 45% for the 5/100/100 wt% HA-DMPE/BN-CNO/DOX formulation and 48% for the formulation without HA-DMPE. These values are comparable to other reported DOX/CNM systems, which typically range from 4% to 65%.[7] Moreover, the 20/100/120 system showed a DRE value of 84%, which is favourable compared to many reported systems where less than 50% of the drug is typically released.[7]

Formulations with low or no HA-DMPE content (5/100/100 and 0/100/100 wt%) exhibit higher DLC values of 45% and 48%, respectively, compared to those with higher HA-DMPE content (20/100/120 and 10/100/120 wt%), which have DLCs of 37% and 36%. This inverse relationship suggests that the HA-DMPE conjugate occupies the pores in the BN-CNOs, leaving less space for DOX binding. The DRE values further support this, showing a direct correlation between HA-DMPE content and DRE—with the 20/100/120 formulation achieving the highest DRE of 84%, highlighting the critical role of HA-DMPE in promoting drug release. This demonstrates that by fine-tuning the HA-DMPE wt% content in the HA-DMPE/BN-CNO/DOX formulation, both DLC and DRE values can be effectively customised.

Notably, the DRE values observed in this study were significantly higher than those from our previous DOX/CNT/HA-DMPE study (~20%).[27] This difference is likely due to the aforementioned filling of the BN-CNO pores by HA-DMPE, preventing DOX from being encapsulated within the pores on the BN-CNO surface. In contrast, encapsulation can often be the case with CNTs.[47] Consequently, in the HA-DMPE/BN-CNO/DOX system, the DOX remains bound to the surface of the BN-CNOs, making it more readily accessible for release.

The drug release behaviour of the various HA-DMPE/BN-CNO/DOX formulations was assessed at both neutral (pH 7.4) and acidic (pH 5.2) conditions, the latter specifically to evaluate the pH-controlled release imparted by the DOX in the system. The cumulative DOX release profiles are reported in Fig. 3 with the corresponding percentage release and standard deviation values, based on triplicate measurements, provided in Table S5.† In addition to having the highest DRE, the 20/100/120 wt% formulation displayed the largest difference in released drug from pH 5.2 to pH 7.4, with a 12-fold increase observed. To investigate whether the remaining bound DOX in the 20/100/120 sample could be liberated in acidic conditions by increasing release time, extended-release studies were per-

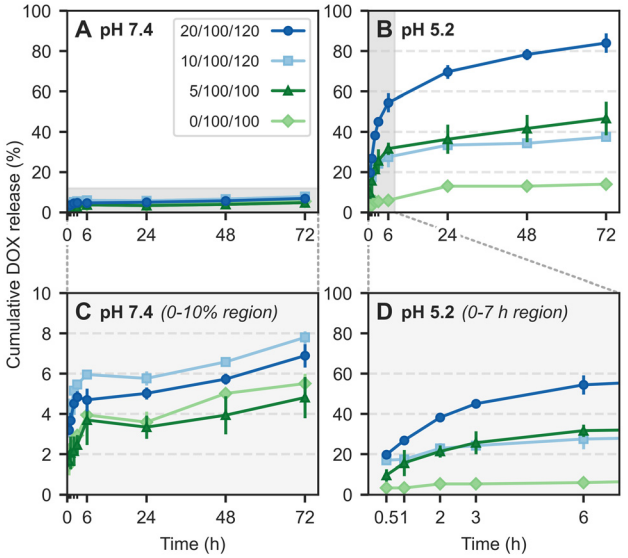

Fig. 3 Drug release studies|Cumulative DOX release profiles over 72 h for 20/100/120, 10/100/120, 5/100/100 and 0/100/100 wt% formulations of the HA-DMPE/BN-CNO/DOX nanocarrier in (A) pH 7.4 buffer (0.01 M PBS), and (B) pH 5.2 buffer (0.01 M sodium acetate). The region marked in grey for the pH 7.4 and pH 5.2 release profiles have been zoomed in (C) & (D), respectively.

formed with 96 h and 120 h time points (Fig. S7†). All the formulations had delayed drug release, which improves the efficacy of the DOX by controlling its kinetic profile. The HA-DMPE-containing formulations displayed an initial DOX burst release within the first 6 h at pH 5.2, this serves to rapidly achieve effective therapeutic concentration of the drug in the target tissue. A slow, sustained release of DOX is then observed for the remaining time points, which could maintain an effective drug concentration in the target tissue. This could prevent efflux of excess DOX from cells, thereby improving its efficacy whilst reducing potential side effects. The concentration of DOX released can be customised by controlling the amount added during loading.

3.4 *In vitro* tests

Three representative cell lines were chosen, namely MCF-7, MDA-MB-468, and MDA-MB-231. Both MDA-MB cell lines were selected to model late-stage, DOX-resistant triple-negative breast cancer (TNBC), and their flow cytometry results (Fig. S8†) confirmed high CD44 receptor expression in both lines (76.1% and 89.3%, respectively). MCF-7 cells were chosen to represent DOX-sensitive breast cancer and were found to express only small amounts of CD44 (2.4%).

The toxicity of the blank (no drug loaded) nanocarrier (20/100 wt% HA-DMPE/BN-CNO) was tested in the three representative cell lines at 24, 48, and 72 h. The cell viability results (Fig. 4A) show that in all cell lines, viability was at least 75% up to a concentration of 15 μg mL^{-1} at 72 h, meaning the DOX-free nanocarrier was non-cytotoxic. There were, however, significant differences between the blank and nanocarrier results, particularly in the MDA-MB cell lines. For example, the viability at 72 h went from 100% (blank) to 81% and 75% for the highest concentration point for MDA-MB-468 and MDA-MB-231, respectively. This could be due to the significant expression of CD44 in both cell lines.

These cytotoxicity results are comparable to our previously published studies on pristine CNOs non-covalently modified with HA-DMPE,[25] as well as CNOs covalently functionalised with a hyaluronic acid through a diamino-PEG linker.[39]

In this study, Caelyx® was used as a standard for comparison in the DOX uptake and anticancer activity assays. To determine the role of CD44 in the nanocarrier's efficacy, two competitive co-incubations were performed, CA (100-fold excess of HA) and CB (CD44 blocking antibody).

In MCF-7 cells with low cell-surface CD44-receptor expression (2.4% positive cells), there was very little difference in uptake from straight drug compared to nanocarrier formulation, with only the 1 μM equivalent DOX concentration point showing any significant difference at 24 h. In this case, both the 10/100/120 and 20/100/120 wt% HA-DMPE/BN-CNO/DOX formulations outperformed DOX alone (by over 25%) and Caelyx® (by over 35%).

As for the MDA-MB-468 cell line, which has a relatively high cell-surface CD44 expression (76.1% positive cells), the 20/100/120 formulation outperformed DOX at the 1 μM concentration point by 27%, and it beat both DOX and Caelyx® at 10 μM equivalent DOX concentration by 39% and 31%, respectively. The most significant improvement in DOX uptake was seen in the highly CD44-expressing MDA-MB-231 cell line (89.3% CD44 positive cells), with the 20/100/120, 10/100/120, and 5/100/100 formulations surpassing DOX at the 10 nM concentration point by 32%, 47%, and 64%, respectively. The same three nanocarriers also outperformed Caelyx® at 100 nM and 1 μM equivalent DOX concentration. At the highest concentration point, the 20/100/120 and 10/100/120 wt% formulations also exceeded both DOX and Caelyx®. The 20/100/120 formulation performed best from a DOX uptake standpoint, imparting over two times the intracellular DOX concentration compared to the drug alone and Caelyx®. Fig. S9† also shows significant uptake improvements over DOX and Caelyx® at 1, 3, and 6 h with various formulations. The addition of CA (co-incubation with competitor) and CB (co-incubation with inhibitor) vastly reduced DOX uptake in the two CD44-expressing MDA-MB cell lines compared to 20/100/120 alone, whilst no significant differences were observed in the MCF-7 cells. For example, DOX uptake at the highest concentration point for the 20/100/120 system was reduced from 1.64 nmol mg^{-1} protein to 0.49 (CA) and 0.48 nmol mg^{-1} protein (CB), proving that the nanocarrier is targeting this receptor and it is essential for HA-DMPE/BN-CNO/DOX uptake.

As for the anticancer effects of the nanocarrier, Fig. 4C reveals no significant differences observed between DOX and nanocarrier at 72 h in MCF-7 cells, even with CA and CB, further highlighting the role of the CD44 receptor. In the MDA-MB-468 cell line, the 20/100/120 formulation reduced cell viability to 72% at the 100 nM concentration, whereas DOX

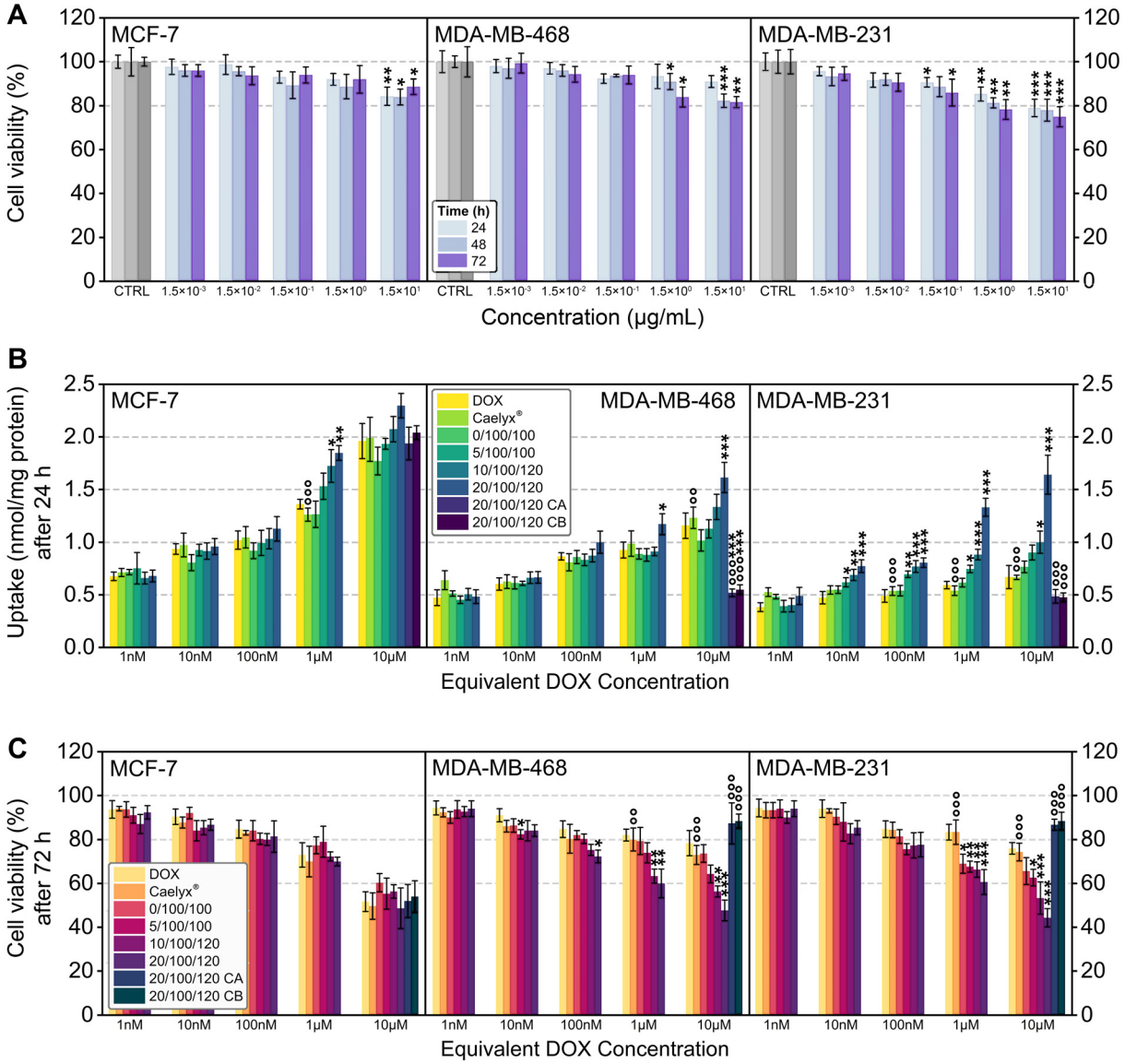

Fig. 4 MCF-7, MDA-MB-468, and MDA-MB-231 cellular uptake and viability|Representative *in vitro* studies, where (A) is MCF-7, MDA-MB-468, and MDA-MB-231 cell viability with varying concentrations of 20/100/0 DOX-free HA-DMPE/BN-CNO system at 24, 48, and 72 h; control studies ('CTRL') are included in all experiments but are only shown here for clarity. (B) Shows cellular uptake studies in MCF-7, MDA-MB-468, and MDA-MB-231 cells at 24 h with DOX, Caelyx®, and varying HA-DMPE/BN-CNO/DOX formulations at a range of equivalent DOX concentrations; and (C) shows MCF-7, MDA-MB-468, and MDA-MB-231 cell viability at 72 h with DOX, Caelyx®, and varying HA-DMPE/BN-CNO/DOX formulations at a range of equivalent DOX concentrations. Statistical significance is indicated as $^{*}p < 0.05$, $^{**}p < 0.01$, $^{***}p < 0.001$ *vs.* DOX, and $^{\circ}p < 0.05$, $^{\circ\circ}p < 0.01$, $^{\circ\circ\circ}p < 0.001$ *vs.* Caelyx®. Competitive co-incubations with excess HA or anti-CD44 blocking antibodies are labelled as CA and CB, respectively.

reduced it to 85%. At both 1 μM and 10 μM, the 20/100/120 and 10/100/120 formulations imparted significant decreases in cell viability compared to DOX and Caelyx®, with the most concentrated 20/100/120 formulation reducing cell viability to 48%, compared to 78% for DOX and 73% for Caelyx®. Again, the most potent anticancer effects were seen in the MDA-MB-231 cell line.

At 1 μM equivalent DOX concentration, all the formulations displayed significant increases in efficacy compared to DOX and Caelyx®, whilst at 10 μM, all the HA-DMPE-containing formulations surpassed DOX and Caelyx®. The 20/100/120 formulation reduced cell viability to 44%, almost half that of DOX alone (76%) and Caelyx® (74%). The addition of CA and CB significantly increased the viability of the MDA-MB cells, whilst minor differences were observed in the MCF-7 cell line; this further highlights the essential role of the CD44 receptor.

The 20/100/120 formulation provided the best uptake and anticancer viability in CD44 expressing cells, particularly in the MDA-MB-231 line at 72 h and 10 μM equivalent DOX concentration. Significant antiproliferative improvements over DOX and Caelyx® were also seen at the shorter incubation times of 24 and 48 h (Fig. S10A and B†).

To further capture the antiproliferative effects of the best-performing system, viability assays for DOX alone and the 20/100/120 wt% formulation (with and without competitive co-incubation) were extended to 96 h and 120 h (Fig. S10C and D†). A significant decrease in viability compared to DOX alone was seen in both MDA-MB cell lines, with MDA-MB-231 cell viability being reduced to just 9% at 10 μM equivalent DOX concentration at 120 h compared to 32% with DOX. Compared to our previous DOX/CNT/HA-DMPE study, the HA-DMPE/BN-CNO/DOX shows significantly improved efficacy compared to the DOX control.[27]

The reduced cell viability was likely attributable to cell necrosis, as indicated by the dose- and time-dependent increase in extracellular LDH. This trend followed the decrease in cell viability induced by DOX, Caelyx®, and the 20/100/120, 10/100/120, and 5/100/100 formulations, with the 20/100/120 wt% formulation surpassing the others (Fig. S11A–E†). Also, necrotic cell death was abrogated by co-incubating the 20/100/120 wt% formulation with an excess of HA or blocking anti-CD44 antibody (Fig. S11A–E†), supporting the hypothesis that the increased cytotoxicity was driven by CD44-mediated endocytosis and resulted from the necrotic action of DOX, the typical mode of cell death elicited by the drug in responsive cells.[48]

Targeting CD44 in TNBC has recently emerged as a promising approach to improve the delivery of DOX in this aggressive tumour. For instance, HA-conjugated photoactivable DOX-loaded poly(lactic-*co*-glycolic acid) (PLGA) nanoparticles (PLGA) nanoparticles (NPs) have successfully increased the drug delivery and the cytotoxic potential against 2D and 3D TNBC cells.[49] Whilst this study achieved a high DLC, their DRE was less than our system's, releasing 42% of bound DOX in 45 h. Similarly, PLGA NPs were used to co-deliver DOX and a prodrug of thymoquinone, which reduces the efflux of DOX *via* P-glycoprotein in TNBC,[50] overcoming the strong chemoresistance often associated with this type of tumour. Whilst high DRE (~100%, 80 h), their DLC was low at 14%. HA-conjugated, poly(ethylenimine)-made NPs have proved their efficacy also when co-loaded with DOX and the FBXO44 CRISPR-KO vector specifically targeting TNBC cancer stem cells *in vitro* and in xenografts.[51] Utilising a dual pH/redox(glutathione) triggered drug release, Wang *et al.* achieved a DRE of 60% and DLC of 14%, both lower than that of our HA-DMPE/BN-CNO/DOX system.

Nanodiamonds (NDs) modified with protamine sulphate and decorated with HA on the outer surface were also loaded with DOX, co-encapsulated with the photosensitiser indocyanine green and the HSP70 small molecule inhibitor apoptozole: these NDs performed better than free DOX when tested against MDA-MB-231 cells subjected to photothermal treatments.[52] Although the co-delivery of multiple drugs is very attractive in oncological-based nanomedicine, it presents a level of complexity and possible undesired drug–drug interaction that may lead to unexpected toxicities or decreased efficacy of DOX in humans. Our system, including biocompatible carbon-based NPs, DOX and HA as key components, simplifies the NPs production and limits the possible occurrence of side effects, increasing at the same time DOX efficacy over the current standard of treatment Caelyx®.

As previously mentioned, cardiotoxicity—primarily driven by apoptosis-mediated cardiomyocyte death and oxidative stress—is a limiting factor in DOX treatments and often increases cancer patient mortality.[6] Indeed, a very recent paper proposed a co-delivery of DOX and cardioprotective agent Saikosaponin A with HA-modified zeolitic imidazolate framework-8 (ZIF-8) nanoparticles that successfully reduced TNBC growth and promotes cardioprotection in Balb/C mice with the murine TNBC 4T1 model.[53] To investigate the ability of HA-DMPE/BN-CNO/DOX to reduce the side effect profile of DOX, cell uptake and viability studies were carried out on AC16 human cardiomyocytes. Cell uptake studies have been carried out at 1, 3, 6 h (Fig. S12A†), and 24 h (Fig. 5A), and cell viability studies have been carried out at 24, 48 h (Fig. S12B†), and 72 h (Fig. 5B). LDH release studies were also carried out in AC16 at 24, 48 and 72 h (Fig. S13†).

The AC16 uptake of the 20/100/120 formulation at 24 h and the highest concentration tested was almost 70% lower than DOX, with no significant differences compared to Caelyx®. At

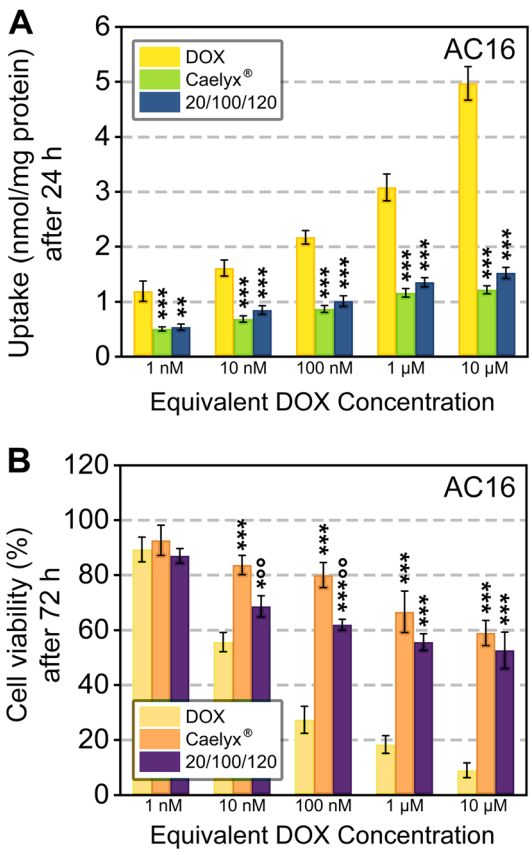

Fig. 5 Human cardiomyocyte studies|AC16 24 h cell uptake (A) and 72 h cell viability (B) with varying concentrations of DOX, Caelyx®, and the 20/100/120 wt% HA-DMPE/BN-CNO/DOX formulation. Statistical significance is indicated as $*p < 0.05$, $**p < 0.01$, $***p < 0.001$ *vs.* DOX, and $°p < 0.05$, $°°p < 0.01$, $°°°p < 0.001$ *vs.* Caelyx®.

72 h and 10 μM equivalent DOX concentration, the AC16 cell viability was 44% higher for the 20/100/120 wt% formulation. Similarly, cell viability for 20/100/120 was significantly higher than DOX for 10 nM, for 1 nM it was comparable to DOX. Although the 20/100/120 cell viability was slightly lower than Caelyx®, the HA-DMPE/BN-CNO/DOX nanocarrier significantly reduces DOX-induced toxicity in human cardiomyocytes (Fig. 5B). This is likely due to AC16 not-expressing the CD44 receptor.[34]

Moreover, LDH release in the AC16 cell line was significantly lower with the 20/100/120 wt% formulation compared to DOX (Fig. S13†). Notably, this reduction was comparable to that observed with Caelyx®, highlighting the reduced side effect profile of our nanocarrier.

3.5 Principal component analysis (PCA)

To determine the effects of varying HA-DMPE content on drug loading and release parameters, principal component analysis (PCA) was performed. The variables are visualised in the biplot in Fig. 6. Two components (PC1 and PC2) were found to account for the majority (96.72%) of variance. Apart from an outlier at the 5% HA-DMPE level, the replicates can be grouped into tight clusters, highlighting the reproducibility of the DOX loading/release procedure. The angle between the DLE and DLC vectors is small, meaning they are closely associated; they also have a strong correlation with the most significant component (PC1), which is primarily a measure of how much DOX is on the nanocarrier. PC1 has a weak negative correlation with pH 5.2 and pH 7.4 DRE, meaning that increasing the amount of DOX on the nanoparticle makes it harder to release all the bound drug.

PC2 accounts for 21.86% of the variance and has a minimal correlation with DLE and DLC. It has a strong positive correlation with DRE at pH 5.2 and a strong negative correlation with pH 7.4 DRE, meaning it primarily measures the effectiveness of the pH-triggered release mechanism. PC2 also correlates with HA-DMPE content, this suggests that in future studies a higher ratio of HA-DMPE could be used to further improve DOX release. The downside to this is that more HA-DMPE means less space on the BN-CNO surface is available for DOX binding, therefore in future studies the amount of HA-DMPE should be finely tuned to optimise these parameters.

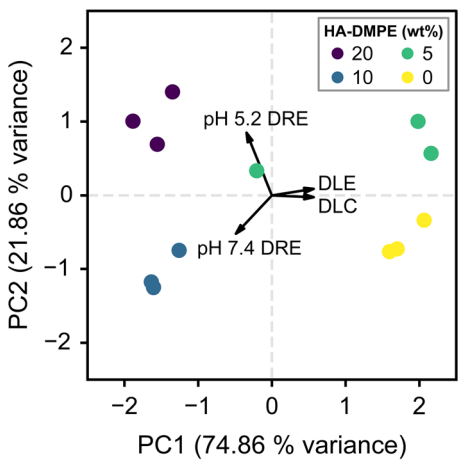

Fig. 6 Principal component analysis|Two-dimensional principal component analysis biplot; line length represents the loading of each variable and the angles between lines represent their correlation.

4. Conclusions

In conclusion, a pH-responsive, CD44-targeted DOX nanocarrier system for the treatment of triple-negative breast cancer has been developed. The system consists of a HA-DMPE conjugate non-covalently bound to BN-CNOs and then loaded with DOX. As the three-component HA-DMPE/BN-CNO/DOX nanocarrier can be formulated at different wt% ratios, we have prepared and evaluated a range of formulations of varying ratios. The nanocarriers were characterised by DLS, ZP, AFM, HRTEM, XPS, FTIR, and UV-vis.

A key finding of this study is that by fine-tuning the wt% ratio of HA-DMPE/BN-CNO/DOX in the formulation, we can optimise therapeutic outcomes. For instance, by adjusting the content of the HA-DMPE component—a bioconjugate designed for targeted drug delivery and improved dispersion of carbon nanomaterials—we observed that we can impart control over both DLC and DRE, as observed in the higher drug release efficiency with increased HA-DMPE content and the inverse relationship between HA-DMPE levels and drug loading capacity. This underscores the potential to optimise therapeutic outcomes by adjusting the HA-DMPE/BN-CNO/DOX formulation wt% composition.

With respect to drug release efficiency, of the various formulations produced, the 20/100/120 wt% HA-DMPE/BN-CNO/DOX ratio was found to have the best drug release efficiency, with 84% of bound drug released after 72 h and a drug loading content of 37%.

In vitro studies were carried out on the DOX-free and DOX-loaded HA-DMPE/BN-CNO/DOX nanocarrier to evaluate their cellular viability, uptake and therapeutic efficacy. The cytotoxicity of the DOX-free nanocarrier was tested in MCF-7, MDA-MB-468, and MDA-MB-231 cell lines, and based on the results it was found to be biocompatible.

The cellular uptake of various HA-DMPE/BN-CNO/DOX formulations was compared to DOX alone and to the liposomal DOX formulation Caelyx®. The 20/100/120 formulation significantly increased DOX uptake and cytotoxic efficacy compared to the drug alone and Caelyx® in both highly CD44-expressing cell lines (MDA-MB-468 and MDA-MB-231).

The role of CD44 in the enhanced uptake of the HA-DMPE-containing formulations was confirmed through competition and inhibition assays with the 20/100/120 wt% formulation. Co-incubation with an excess of HA as a competitor (CA) or an anti-CD44 blocking antibody as an inhibitor (CB) significantly reduced uptake in the highly CD44-expressing MDA-MB-468 and MDA-MB-231 cells, while having minimal effect in the low CD44-expressing MCF-7 cells. The cell viability studies mir-

rored these findings, showing that the DOX-loaded 20/100/120 wt% formulation had minimal effect on viability when CA or CB was added. Moreover, the cytotoxic efficacy of the DOX-loaded formulations increased in proportion to their wt% HA-DMPE content.

Notably, the cellular uptake and cytotoxicity of the nanocarrier system in AC16 human cardiomyocytes showed significant improvements over DOX and were comparable to Caelyx®. At the highest concentration tested, uptake of the 20/100/120 wt% formulation was nearly 70% lower than DOX, while at 72 h, cell viability was 44% higher than with DOX, demonstrating a considerable reduction in cardiotoxicity.

In summary, this study demonstrates the development of a pH-responsive, CD44-targeted HA-DMPE/BN-CNO/DOX nanocarrier for the treatment of triple-negative breast cancer (TNBC). Through careful optimisation of the HA-DMPE/BN-CNO/DOX wt% ratios, the 20/100/120 formulation exhibited superior drug release efficiency, enhanced cellular uptake, and increased cytotoxic efficacy compared to DOX alone and Caelyx®, particularly in highly CD44-expressing cancer cells. Selectivity towards CD44-expressing cells was confirmed through competition and inhibition assays. Importantly, the nanocarrier also demonstrated a reduced cardiotoxicity profile in human cardiomyocytes compared to DOX alone. Future work will focus on elucidating the mechanism of TNBC cell death, which could aid our understanding of how the nanocarrier overcomes DOX resistance, and further optimising the formulation to enhance therapeutic outcomes.

Author contributions

Hugh Mohan: data curation, formal analysis, investigation, methodology, validation, visualization, writing – original draft. Iris Chiara Salaroglio: investigation, validation. Michał Bartkowski: data curation, visualization, writing – review & editing. Kellyjean Courtney: investigation, validation. Ilaria Andreana: investigation. Tania Limongi: investigation. Raul Arenal: investigation, funding acquisition, writing – review & editing. Chiara Riganti: data curation, investigation, methodology, supervision, validation, writing – review & editing. Silvia Arpicco: conceptualization, methodology, project administration, supervision, writing – review & editing. Silvia Giordani: conceptualization, methodology, project administration, supervision, writing – review & editing, funding acquisition.

Abbreviations

AFM	Atomic force microscopy
BN-CNO	Boron/nitrogen doped carbon nano-onion
CNM	Carbon nanomaterial
CNT	Carbon nanotube
CA	Co-incubation with CD44 competitor
CB	Co-incubation with CD44 inhibitor
DOX	Doxorubicin
DLC	Drug loading content
DLE	Drug loading efficiency
DRE	Drug release efficiency
DLS	Dynamic light scattering
HAADF-STEM	High-angle annular dark-field scanning transmission electron microscopy
HRTEM	High-resolution transmission electron microscopy
HA-DMPE	Hyaluronic acid-1,2-dimyristoyl-*sn-glycero*-3-phosphoethanolamine
PBS	Phosphate-buffered saline
TNBC	Triple-negative breast cancer
XPS	X-ray photoelectron spectroscopy.

Data availability

The data supporting this article have been included as part of the ESI.†

Conflicts of interest

The authors declare that they have no known competing financial interests or personal relationships that could have appeared to influence the work reported in this paper.

Acknowledgements

This work was supported by Science Foundation Ireland (22/FFP-A/11067). Financial support from the Irish Research Council (GOIPG/2021/210 to H. M.), from the School of Chemical Sciences (SCS) at DCU (research assistantship to K. C.), from the Italian Ministry of University and Research (PRIN 2022ZBZFX3 to S. A. and C. R.) and from the Italian Association for Cancer Research (IG29250 to C. R.) are gratefully acknowledged. R. A. acknowledges funding from the Government of Aragon (DGA) through the project E13_23R, the Spanish MICIU with funding from European Union Next Generation EU (PRTR-C17.I1) promoted by the Government of Aragon and by the Spanish MICIU (PID2019-104739GB-100/AEI/10.13039/501100011033, PID2023-151080NB-I00/AEI/10.13039/501100011033 and CEX2023-001286-S MICIU/AEI 10.13039/501100011033). The TEM and XPS works were conducted in the Laboratorio de Microscopias Avanzadas (LMA) at the Universidad de Zaragoza. AFM and UV-vis absorption spectroscopy was performed in the Nano Research Facility (NRF) in DCU. DLS, ZP, and FTIR spectroscopy was performed at the SCS, DCU. This article is based upon work from COST Action CA21126 - Carbon molecular nanostructures in space (NanoSpace), supported by COST (European Cooperation in Science and Technology).

References

1 Breast cancer, **https://www.who.int/news-room/fact-sheets/detail/breast-cancer**, accessed June 20, 2024.

2 K. Aysola, A. Desai, C. Welch, J. Xu, Y. Qin, V. Reddy, R. Matthews, C. Owens, J. Okoli, D. J. Beech, C. J. Piyathilake, S. P. Reddy and V. N. Rao, *Hered. Genet.*, 2013, **2013**, 001.
3 G. Arora, S. Ghosh and S. Chatterjee, *Explor. Target. Anti-tumor Ther.*, 2021, **2**, 208–226.
4 J. L. Nitiss, *Nat. Rev. Cancer*, 2009, **9**, 338–350.
5 K. Johnson-Arbor and R. Dubey, *StatPearls*, StatPearls Publishing, Treasure Island (FL), 2022.
6 P. S. Rawat, A. Jaiswal, A. Khurana, J. S. Bhatti and U. Navik, *Biomed. Pharmacother.*, 2021, **139**, 111708.
7 H. Mohan, A. Fagan and S. Giordani, *Pharmaceutics*, 2023, **15**, 1545.
8 J. Bartelmess and S. Giordani, *Beilstein J. Nanotechnol.*, 2014, **5**, 1980–1998.
9 Y. Liu, Y. Pu, L. Sun, H. Yao, B. Zhao, R. Zhang and Y. Zhang, *J. Biomed. Nanotechnol.*, 2016, **12**, 1393–1403.
10 D. S. Randive, A. S. Gavade, K. P. Shejawal, M. A. Bhutkar, S. D. Bhinge and N. R. Jadhav, *Drug Dev. Ind. Pharm.*, 2021, **47**, 1401–1412.
11 S. Kaur, N. K. Mehra, K. Jain and N. K. Jain, *Artif. Cells, Nanomed., Biotechnol.*, 2017, **45**, 242–250.
12 D. Salas-Treviño, O. Saucedo-Cárdenas, M. D. J. Loera-Arias, H. Rodríguez-Rocha, A. García-García, R. Montes-de-Oca-Luna, E. I. Piña-Mendoza, F. F. Contreras-Torres, G. García-Rivas and A. Soto-Domínguez, *Nanomaterials*, 2019, **9**, 1572.
13 N. Vahedi, F. Tabandeh and M. Mahmoudifard, *Biotechnol. Appl. Biochem.*, 2022, **69**, 1068–1079.
14 S. Shan, S. Jia, T. Lawson, L. Yan, M. Lin and Y. Liu, *IJMS*, 2019, **20**, 4454.
15 A. A. Bhirde, V. Patel, J. Gavard, G. Zhang, A. A. Sousa, A. Masedunskas, R. D. Leapman, R. Weigert, J. S. Gutkind and J. F. Rusling, *ACS Nano*, 2009, **3**, 307–316.
16 K. Ajima, M. Yudasaka, T. Murakami, A. Maigné, K. Shiba and S. Iijima, *Mol. Pharmaceutics*, 2005, **2**, 475–480.
17 H. Huang, M. Liu, J. Chen, L. Mao, G. Zeng, Y. Wen, J. Tian, N. Zhou, X. Zhang and Y. Wei, *J. Taiwan Inst. Chem. Eng.*, 2018, **86**, 192–198.
18 M. Xie, F. Zhang, L. Liu, Y. Zhang, Y. Li, H. Li and J. Xie, *Appl. Surf. Sci.*, 2018, **440**, 853–860.
19 X. Zhang, S. Wang, C. Fu, L. Feng, Y. Ji, L. Tao, S. Li and Y. Wei, *Polym. Chem.*, 2012, **3**, 2716–2719.
20 Z. Li, J. Ni, L. Liu, L. Gu, Z. Wu, T. Li, K. I. Ivanovich, W. Zhao, T. Sun and T. Wang, *ACS Appl. Mater. Interfaces*, 2021, **13**, 29340–29348.
21 J. M. González-Domínguez, L. Grasa, J. Frontiñán-Rubio, E. Abás, A. Domínguez-Alfaro, J. E. Mesonero, A. Criado and A. Ansón-Casaos, *Colloids Surf., B*, 2022, **212**, 112363.
22 M. Das, S. R. Datir, R. P. Singh and S. Jain, *Mol. Pharmaceutics*, 2013, **10**, 2543–2557.
23 H. Lai, M. Lu, H. Lu, M. H. Stenzel and P. Xiao, *Polym. Chem.*, 2016, **7**, 6220–6230.
24 Y. Zhou, K. Vinothini, F. Dou, Y. Jing, A. A. Chuturgoon, T. Arumugam and M. Rajan, *Arabian J. Chem.*, 2022, **15**, 103649.
25 M. d'Amora, A. Camisasca, A. Boarino, S. Arpicco and S. Giordani, *Colloids Surf., B*, 2020, **188**, 110779.
26 H. Mohan, V. Bincoletto, S. Arpicco and S. Giordani, *Materials*, 2022, **15**, 5987.
27 S. Arpicco, M. Bartkowski, A. Barge, D. Zonari, L. Serpe, P. Milla, F. Dosio, B. Stella and S. Giordani, *Front. Chem.*, 2020, **8**, 578008.
28 S. Sturari, I. Andreana, P. Aprà, V. Bincoletto, J. Kopecka, L. Mino, B. Zurletti, B. Stella, C. Riganti, S. Arpicco and F. Picollo, *Nanoscale*, 2024, **16**, 11610–11622.
29 K.-W. Lan, W.-Y. Huang, Y.-L. Chiu, F.-T. Hsu, Y.-C. Chien, Y.-Y. Hsiau, T.-W. Wang and P. Y. Keng, *Biomater. Adv.*, 2023, **155**, 213699.
30 Y. Feng, S. Lu, Q. Zhao, T. Sun, Y. Shi, G. Gao, H. Wang and J. Zhi, *ACS Appl. Nano Mater.*, 2024, **7**(7), 7008–7017.
31 M. d'Amora, A. Camisasca, R. Arenal and S. Giordani, *Nanomaterials*, 2021, **11**, 3017.
32 A. Camisasca, A. Sacco, R. Brescia and S. Giordani, *ACS Appl. Nano Mater.*, 2018, **1**, 5763–5773.
33 A. Vadhan, M.-F. Hou, P. Vijayaraghavan, Y.-C. Wu, S. C.-S. Hu, Y.-M. Wang, T.-L. Cheng, Y.-Y. Wang and S.-S. F. Yuan, *Biomedicines*, 2022, **10**, 2488.
34 Tissue expression of CD44 - Staining in heart muscle - The Human Protein Atlas, **https://www.proteinatlas.org/ENSG00000026508-CD44/tissue/heart+muscle**, accessed June 21, 2024.
35 P. Swietach, R. D. Vaughan-Jones, A. L. Harris and A. Hulikova, *Philos. Trans. R. Soc., B*, 2014, **369**, 20130099.
36 European Medicines Agency, EMA/635791/2019, 2020.
37 A. A. Gabizon, S. Gabizon-Peretz, S. Modaresahmadi and N. M. La-Beck, *BMJ Oncol.*, 2025, **4**, e000573.
38 Z.-M. Zhang, S. Chen and Y.-Z. Liang, *Analyst*, 2010, **135**, 1138–1146.
39 M. Bartkowski, V. Bincoletto, I. C. Salaroglio, G. Ceccone, R. Arenal, S. Nervo, B. Rolando, C. Riganti, S. Arpicco and S. Giordani, *J. Colloid Interface Sci.*, 2024, **659**, 339–354.
40 C. Riganti, I. C. Salaroglio, V. Caldera, I. Campia, J. Kopecka, M. Mellai, L. Annovazzi, A. Bosia, D. Ghigo and D. Schiffer, *Neuro. Oncol.*, 2013, **15**, 1502–1517.
41 R. K. Khangarot, A. Bhatnagar and G. Pemawat, in *Polymer Blend Nanocomposites for Energy Storage Applications*, ed. S. Thomas, A. R. Ajitha and M. Jaroszewski, Elsevier, 2023, pp. 293–310.
42 D. Schild, S. Ulrich, J. Ye and M. Stüber, *Solid State Sci.*, 2010, **12**, 1903–1906.
43 P. Lazar, R. Mach and M. Otyepka, *J. Phys. Chem. C*, 2019, **123**, 10695–10702.
44 S. Y. Kim, J. Park, H. C. Choi, J. P. Ahn, J. Q. Hou and H. S. Kang, *J. Am. Chem. Soc.*, 2007, **129**, 1705–1716.
45 R. Augustine, A. Hasan, R. Primavera, R. J. Wilson, A. S. Thakor and B. D. Kevadiya, *Mater. Today Commun.*, 2020, **25**, 101692.
46 S. Behzadi, V. Serpooshan, W. Tao, M. A. Hamaly, M. Y. Alkawareek, E. C. Dreaden, D. Brown, A. M. Alkilany,

O. C. Farokhzad and M. Mahmoudi, *Chem. Soc. Rev.*, 2017, **46**, 4218–4244.
47 L. Contreras, I. Villarroel, C. Torres and R. Rozas, *Molecules*, 2021, **26**, 1586.
48 C. Riganti, E. Gazzano, G. R. Gulino, M. Volante, D. Ghigo and J. Kopecka, *Cancer Lett.*, 2015, **360**, 219–226.
49 S. Gómez-Pastor, A. Maugard, H. R. Walker, J. Elies, K. E. Børsum, G. Grimaldi, G. Reina and A. Ruiz, *Colloids Surf., B*, 2025, **249**, 114504.
50 M. Bhattacharjee, A. Ghosh, S. Das, S. Sarker, S. Bhattacharya, A. Das, S. Ghosh, S. Chattopadhyay, S. Ghosh and A. Adhikary, *ACS Biomater. Sci. Eng.*, 2024, **10**, 6314–6331.
51 T. Wang, T. Chen, D. Li, X. Hang, S. Zhang, H. Yi, T. Jiang, D. Ding and X. Zhang, *J. Controlled Release*, 2025, **378**, 1080–1091.
52 X. Cui, Z. Liang, J. Lu, X. Wang, F. Jia, Q. Hu, X. Xiao, X. Deng, Y. Wu and W. Sheng, *Nanoscale*, 2021, **13**, 13375–13389.
53 D. Li, Y. Yao, K. Wang, C. Lei, X. Peng, C. Cao, K. Zhu, Z. Zhu and F. Shao, *Biomater. Adv.*, 2025, **167**, 214114.